Check for updates

Natural assembly of a ternary Ag–SnS–TiO₂ photocatalyst and its photocatalytic performance under simulated sunlight

Yunhong Jiang,†[a] Zhongmei Yang,†[a] Ping Zhang,*[a] Haibao Jin [b]
and Yanhuai Ding [*a]

Natural assembly method was utilized to prepare a novel ternary Ag–SnS–TiO₂ nanocomposite, in which TiO₂ nanobelts were used as templates. The co-loading of Ag and SnS nanoparticles endows TiO₂ nanobelts with enhanced photocatalytic capability, resulting from the broadened light absorption spectra and decreased band gaps. Comparing with raw TiO₂ nanobelts and commercial Degussa P25, an improvement in photodegradation of simulated organic pollutants was successfully demonstrated due to the decreasing recombination of photogenerated electron–hole pairs. Our work presents a new strategy for the preparation of ternary TiO₂-based photocatalysts in the practical application of wastewater treatment.

1. Introduction

With the growth of population and urbanization, the energy crisis and environmental pollution have emerged as two urgent challenges. Consequently, development of clean and sustainable alternative energy sources has attracted more and more attention, due to the decreasing availability of fossil fuels.[1,2] Another effective strategy is to discover an adaptable catalyst to degrade the pre-existing contaminants. In developing countries, the ubiquitous release of organic pollutants including dyes, pigments, drugs, saturated hydrocarbons, aromatic compounds insecticides, and pesticides in the water resources is posing an irreversible problem to the environments and ecosystem. Owing to the green, benign, and cost effective properties, heterogeneous photocatalysts such as TiO₂, ZnO, Fe₂O₃, CdS, ZnS, SnO₂, Bi₂O₃, V₂O₅ have been widely developed for efficient photodegradation of various harmful organic pollutants in the wastewater. In particular, TiO₂ has attracted growing attentions due to its abundant reserves, low cost, non-toxicity, good light stability and high UV photocatalytic (PC) activity in nature.[3–7] Nevertheless, the extensive practical applications of TiO₂ are highly impeded by the unexpected diminishment of PC degradation efficiency resulted from certain factors such as electron (e⁻)/hole (h⁺) recombination. In addition, the wide band gap (3.2 eV) prohibits TiO₂ to efficiently absorb the solar light, leading to low light utilization efficiency (less than 5%).[8,9] Two

significant strategies has been presented to overcome these drawbacks,[6] which are coupling TiO₂ with other semiconductors and addition of hybrid dopants (*e.g.*, hydrogenation, noble metal modification and transition metals).[10] The utility of semiconductors with narrower band gaps to fabricate TiO₂-based P–N heterostructures is a reasonable method to improve the performance of TiO₂. The P–N heterojunction not only creates a potential gradient at the junction interface, but also transfers electrons from the excited narrow-band gap semiconductor to another adhesion layer, in order to promote the light utilization efficiency. Therefore, a series of semiconductor quantum dots (QDs) have been widely used as photosensitizers to form P–N heterojunction then improve the utilization efficiency of solar energy.[11–13] In particular, stannous sulfide (SnS), a typical p-type semiconductor material, possesses narrow direct band gap (1.3 eV) and indirect band gap (1.09 eV), exhibiting excellent performance in solar absorption and photocatalysis.[14,15] As expected, SnS–TiO₂ binary composite provides an effective platform to significantly improve the electron transport properties.[15,16] Besides, addition of hybrid dopants is another effective method to promote the PC efficiency, owing to the good advantages on lower Fermi energy level and light absorption in visible region.[17–22] In particular, Ag–TiO₂ binary composite has received great attention in recent years, due to the direct sunlight PC activity and excellent chemical stability.[19] The PC activity of Ag–TiO₂ binary composite can be tuned by regulating nanoparticle loading, dispersion, shape, size and metal–support interaction.[23] Lu *et al.*[24] have prepared Ag–TiO₂ nanorods by UV irradiation, exhibiting higher electron transport efficiency than that of pure TiO₂ nanorods. Yang *et al.* have reported that Ag–TiO₂ nanotube heterojunction possessed higher photocatalytic activity than

[a]*College of Civil Engineering and Mechanics, Xiangtan University, Xiangtan, 411105, PR China. E-mail: zhangp@xtu.edu.cn; yhding@xtu.edu.cn*

[b]*Department of Chemistry, University of North Carolina at Chapel Hill, North Carolina 27599, USA*

† The first two authors contributed equally to this work.

pure TiO_2 nanotubes.[9] Herein, we firstly propose a new design of ternary Ag–SnS–TiO_2 nanobelts photocatalyst prepared from TiO_2 NBs. The obtained ternary nanocomposite showed broader visible light absorption and higher PC activity than the pristine TiO_2 NBs and commercial P25, owing to the synergetic effects from Ag and SnS nanoparticles.
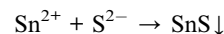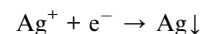
2. Experimental section

2.1 Materials

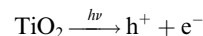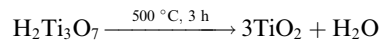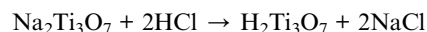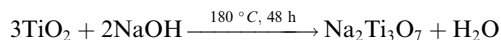TiO_2 (Degussa, P-25), sodium hydroxide (NaOH), hydrochloric acid (HCl), sodium sulfide (NaS), stannous chloride dihydrate ($SnCl_2 \cdot 2H_2O$), silver nitrate ($AgNO_3$), nitric acid (HNO_3), ethanol (C_2H_5OH), methylene blue (MB), carbon tetrachloride (CCl_4) and rhodamine B (RHB) were purchased from Sinopharm Chemical Co., Ltd. without further purification.

2.2 Preparation of TiO_2 NBs

In a typical reaction, 0.3 g of P25 was mixed with 80 mL of 10 M NaOH aqueous solution. The mixture was transferred to a 100 mL Teflon-lined stainless steel autoclave. Followed by heating at 180 °C for 48 hours, the mixture was air cooled to room temperature. The obtained dispersion was filtered and thoroughly washed with deionized water for five times. The wet powder was immersed in 200 mL of 0.1 M HCl aqueous solution, stirring for 24 hours. Followed by washing with distilled water, the obtained $H_2Ti_3O_7$ precursors were annealed at 500 °C for 3 hours to prepare bare TiO_2 NBs.

2.3 Preparation of Ag–SnS–TiO_2 NBs

Ternary Ag–SnS–TiO_2 NBs were fabricated by natural assembly from photo-reduction technology[25,26] and SILAR method,[27,28] as shown in Fig. 1. Raw TiO_2 NBs were synthesized by a alkali-hydrothermal method by using commercially available TiO_2 (Degussa, P-25) as the titanium source.[29] To facilitate the adsorption of Ag nanoparticles and deposition of SnS nano-particles, hydroxyl groups were introduced onto the surface of TiO_2 NBs, through soaking the nanobelts in concentrated nitric acid.[30] The hydroxyl groups not only benefit the deposition of SnS and Ag, but also prevent the aggregation of nanoparticles. Following, Ag nanoparticles are decorated on TiO_2 NBs after a moderate photo-reductive deposition. Followed by doping SnS onto the Ag–TiO_2 NBs by SILAR method, the ternary Ag–SnS–TiO_2 NBs were successfully synthesized. The overall reactions in each procedure can be described as follows:

Fig. 1 Assembly procedure for preparation of Ag–SnS–TiO_2 NBs.

$$3TiO_2 + 2NaOH \xrightarrow{180\,°C,\,48\,h} Na_2Ti_3O_7 + H_2O$$

$$Na_2Ti_3O_7 + 2HCl \rightarrow H_2Ti_3O_7 + 2NaCl$$

$$H_2Ti_3O_7 \xrightarrow{500\,°C,\,3\,h} 3TiO_2 + H_2O$$

$$TiO_2 \xrightarrow{h\nu} h^+ + e^-$$

$$Ag^+ + e^- \rightarrow Ag\downarrow$$

$$Sn^{2+} + S^{2-} \rightarrow SnS\downarrow$$

In a typical procedure, 0.2 g of TiO_2 NBs was soaked in 100 mL of 10 M concentrated nitric acid for 1 hour, to introduce a large amount of hydroxyl groups onto the surface of TiO_2 NBs. Ag nanoparticles are decorated on TiO_2 NBs by constant ultra-violet light deposition. 0.2 g of TiO_2 NBs and 100 mL of 0.001 M $AgNO_3$ solution were mixed together, stirring and exposing to under a high-pressure mercury lamp for 6 hours. The power of the high-pressure mercury lamp is 300 W, and the distance between the solution and the lamp is 20 cm. Following, the samples are rinsed with ultrapure water and dried at 60 °C for 12 hours to obtain Ag–TiO_2 NBs. SnS is deposited on Ag–TiO_2 NBs by a modified successive ion layer absorption and reaction technique (SILAR) method.[31] First, 0.2 g of Ag–TiO_2 NBs was immersed in 100 mL of 1 M $SnCl_2$ solution for 10 min and rinsed with ultrapure water and filtered, followed by rinsing with 200 mL of 1 M Na_2S solution. After washing with ultrapure water and filtrating, the SILAR process was repeated 6 times to obtain Ag–SnS–TiO_2 NBs precursors. Then, the precursor was sintered in an argon atmosphere (>99.9%) at 500 °C for 2 hours to prepare the final ternary Ag–SnS–TiO_2 NBs.

2.4 PC activity test

Methylene blue (MB) (3.0×10^{-5} mol L^{-1}, 100 mL, pH ≈ 6.0) and rhodamine B (RHB) (3.0×10^{-5} mol L^{-1}, 100 mL, pH ≈ 6.0) were used as representative dye indicators to evaluate PC activity of Ag–SnS–TiO_2 photocatalysts. Taking MB as an example, 20 mg of ternary Ag–SnS–TiO_2 NBs photocatalyst was dispersed ultrasonically in MB aqueous solution and sonicated in the dark for 10 minutes to ensure the establishment of adsorption/desorption equilibrium. The mixture was loaded into a glass cylindrical jacketed vessel and exposed to a 300 W metal halide lamp, continuously agitating with an irradiation distance of 25 cm and an irradiation area of 31 cm^2. The entire PC reaction is carried out at room temperature with vigorous stirring and water cooling. About 3.0 mL aliquot was removed at a given time interval and the catalyst was separated from the suspension by filtration through a 0.22 μm cellulose membrane. The PC degradation process was monitored by UV-vis spectro-photometer (Lambda 950; measurement of MB absorption at
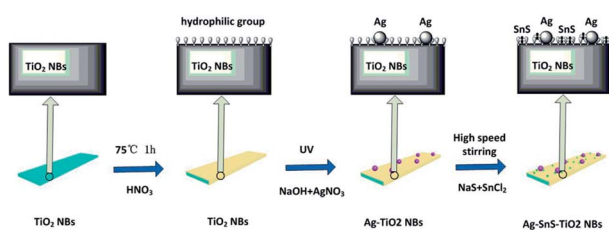
664 nm; measurement of RHB absorption at 552 nm). Comparative experiments with electron (e^-) or hole (h^+) trapping agents were performed in the same manner except that 20 mL of ethanol or carbon tetrachloride were added.

2.5 Characterization

The phase and microstructure of the samples were investigated by Raman spectroscopy, X-ray diffraction (XRD), high resolution transmission electron microscopy (HRTEM) and X-ray photoelectron spectroscopy (XPS). Raman spectroscopy was performed using a Renishaw in *via* microscope with 488 nm Ar ion laser and an excitation wavelength of 325 nm. The morphology of Ag–SnS–TiO$_2$ NBs and bare TiO$_2$ NBs was evaluated using a JEOL JEM-2100 TEM at an accelerating voltage of 200 kV. Photoluminescence (PL) spectra were measured by a FP-6500 fluorescence spectrophotometer (JASCO, Japan) with an excitation wavelength of 325 nm. Powder XRD measurements were performed on a Bruker D8 Advance Powder X-ray diffractometer with CuKα ($\lambda = 0.15406$ nm). The resulting diffraction pattern was collected from 20° to 80° at a scan rate of 1.5° min^{-1}. X-ray photoelectron spectroscopy (XPS) measurements were collected using a VG Scientific ESCALAB 250 instrument using an aluminum Kα X-ray radiation source ($h = 1486.6$ eV). For all scans, high resolution spectra were collected at a residence time of 0.1 s per point. The scans were measured by energy harvest at 50 eV and a separate sweep by energy at 20 eV.

3. Results and discussion

TEM and HRTEM were performed to elaborately observe the morphology change from pure TiO$_2$ NBs to ternary Ag–SnS–TiO$_2$ NBs (Fig. 2). Some ribbon-like TiO$_2$ nanobelts with a length of
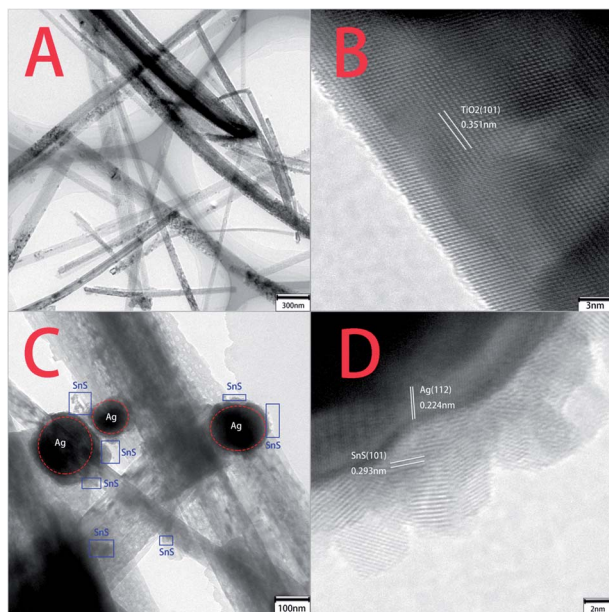
Fig. 2 TEM and HRTEM images of pristine TiO$_2$ NBs and ternary Ag–SnS–TiO$_2$ NBs. (A and B) Pristine TiO$_2$ NBs; (C and D) ternary Ag–SnS–TiO$_2$ NBs.
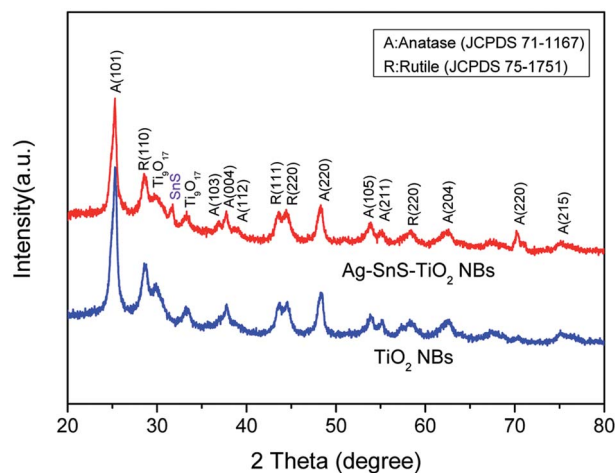
Fig. 3 XRD spectra of ternary Ag–SnS–TiO$_2$ NBs and pristine TiO$_2$ NBs.

several micrometers were clearly found in the low resolution TEM image (Fig. 2A). Measured from the high resolution TEM image (Fig. 2B), a lattice spacing of 0.351 was ascribed to the (101) planes of TiO$_2$ crystal anatase phase.[19] Recent investigation demonstrated that (101) facet of anatase crystals exhibited higher reactivity than (001) facet in photo-oxidation reactions for ˙OH radical generation.[32] Fig. 2C and D showed representative TEM images of ternary Ag–SnS–TiO$_2$ NBs, indicating the successful preparation of ternary nanocomposite. The nanocomposite consists of Ag and SnS nanoparticles with the diameters from several nanometers to over one hundred nanometers. The lattice fringes of Ag and SnS nanoparticles can be measured in the HRTEM image (Fig. 4D). The 0.224 nm and 0.293 nm lattice spacing were assigned to the (112) plane of Ag nanoparticle and (101) plane of SnS nanoparticle, respectively.[19,33] Ag and SnS nanoparticles were firmly anchored on the surface of TiO$_2$ NBs, where the hydrophilic groups serve as anchoring sites. In the nanocomposite, the coordination
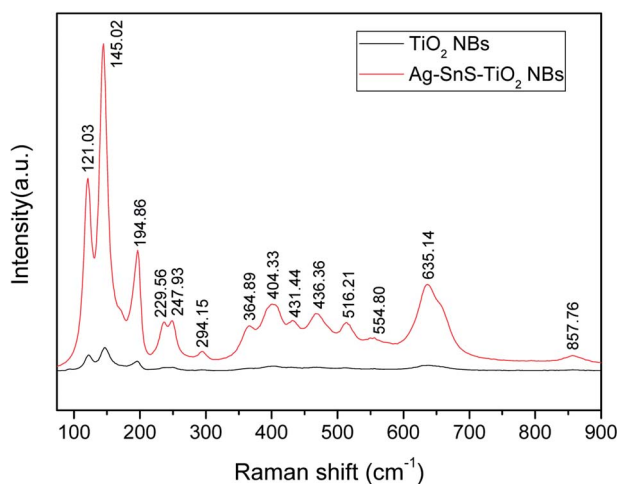
Fig. 4 Raman spectra of ternary Ag–SnS–TiO$_2$ NBs (red curve) and pristine TiO$_2$ NBs (black curve).
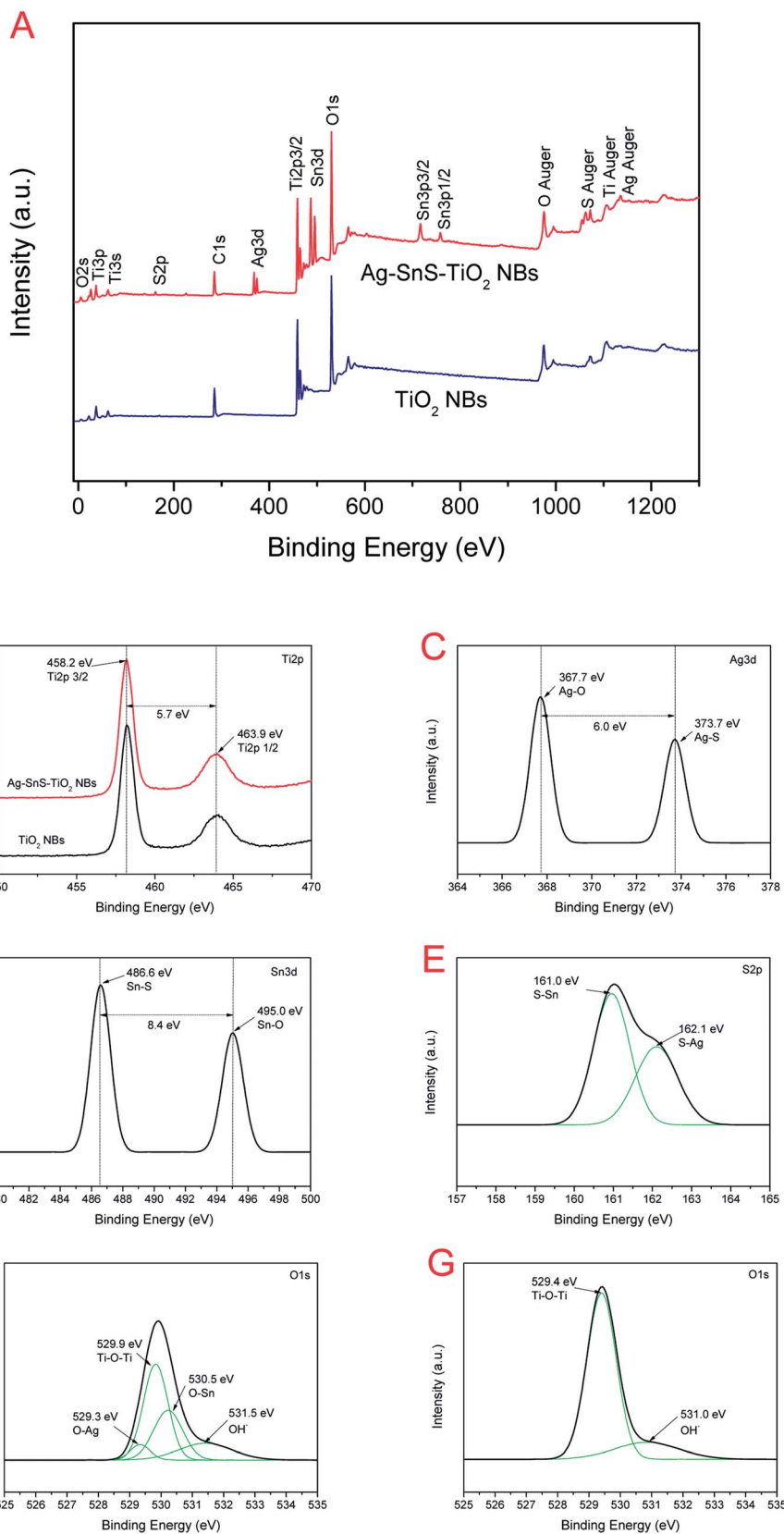
Fig. 5 (A) Full scanning spectra of Ag–SnS–TiO$_2$ NBs and TiO$_2$ NBs; (B) Ti 2p fine XPS spectra of Ag–SnS–TiO$_2$ NBs and TiO$_2$ NBs; (C) Ag 3d fine XPS spectra of Ag–SnS–TiO$_2$ NBs; (D) Sn 3d spectrum of Ag–SnS–TiO$_2$ NBs; (E) S 2p fine XPS spectra of Ag–SnS–TiO$_2$ NBs; (F) O 1s XPS spectra of Ag–SnS–TiO$_2$ NBs; (G) O 1s Fine XPS spectra of TiO$_2$ NBs.

interaction of hydrophilic groups may hinder the nanoparticles from agglomeration and enable an even distribution on the TiO_2 NBs, whilst the nanoparticles may serve as stabilizers to prevent the TiO_2 NBs from aggregation.

The structural information and purity of Ag–SnS–TiO_2 NBs were further characterized by XRD (Fig. 3). The diffraction peaks at $2\theta = 25.3°$, $37.7°$, $48.0°$, $53.8°$, $54.9°$ and $62.6°$ were ascribed to the anatase phase of TiO_2 (JCPDS, 71-1167). Meanwhile, the characteristic peaks at $2\theta = 29.8°$ and $33.3°$ corresponded to the reduction phase (Ti_9O_{17}) of rutile phase (JCPDS 75-1751), indicating the interaction of SnS and the rutile phase.[29] Besides, the diffraction peak of the SnS (101) crystal plane was found at $2\theta = 31.5°$, indicating the presence of SnS nanoparticles (JCPDS, 83-1758). The diffraction peak of the SnS (101) crystal plane at $2\theta = 30.5°$ (JCPDS, 83-1758) may overlap with the diffraction peak of Ti_9O_{17} at $2\theta = 29.8°$. The diffraction peak at $2\theta = 37.8°$ assigned to the (112) plane of Ag nanoparticles have overlapped with diffraction peak of (103) plane in the anatase phase of TiO_2. However, the notable enhancement of shoulder peak indicated the *in situ* loading of Ag nanoparticles. Therefore, XRD spectra demonstrated the successful formation of ternary Ag–SnS–TiO_2 NBs.

Raman spectroscopy provided further evidence for the ornaments of Ag and SnS nanoparticles on TiO_2 NBs. As shown in Fig. 4, the strong scattering bands at 145 cm^{-1}, 404 cm^{-1}, 516 cm^{-1} and 635 cm^{-1} were ascribed to the anatase phase. Another two scattering bands at 229 cm^{-1} and 294 cm^{-1} were ascribed to the rutile phase, in good agreement with the XRD result. Strong scattering bands of the SnS (101) crystal plane were found at about 195 cm^{-1}, indicating the presence of SnS nanoparticles. Notably, the strong scattering bands at 121 cm^{-1} and 248 cm^{-1} were attributed to the formation of chemical bonds among Ag, SnS and TiO_2, lattice defects or disorders.[34]

XPS was also employed to analyze the information on the surface electronic state and the composition of ternary Ag–SnS–TiO_2 NBs (Fig. 5). The fully scanned spectrum of ternary nanocomposite displayed in Fig. 5A, showing the presence of multiple elements in the TiO_2 and Ag–SnS–TiO_2 NBs. C signals in TiO_2 and Ag–SnS–TiO_2 NBs were attributed to carbon-based contaminants from the atmosphere or the vacuum system. The magnified XPS spectra exhibited elaborate surface binding energy (BE) of ternary Ag–SnS–TiO_2 NBs (Fig. 5B–G). Two signals at 463.9 eV and 458.2 eV may stem from Ti 2p1/2 and Ti 2p3/2 (Fig. 5B), respectively, characteristic of TiO. The binding energy between Ti 2p1/2 and Ti 2p3/2 is 5.7 eV, which can be considered as the normal state of Ti^{4+} in Ag–SnS–TiO_2 NBs. The signal of Ti 2p in Ag–SnS–TiO_2 slightly shifted compared to that in TiO_2 NBs, which can be ascribed to the formation of Ti_9O_{17}.[29] Fig. 5C shows a high resolution XPS spectrum of Ag 3d in Ag–SnS–TiO_2 NBs. Two signals at 373.7 eV and 486.6 eV
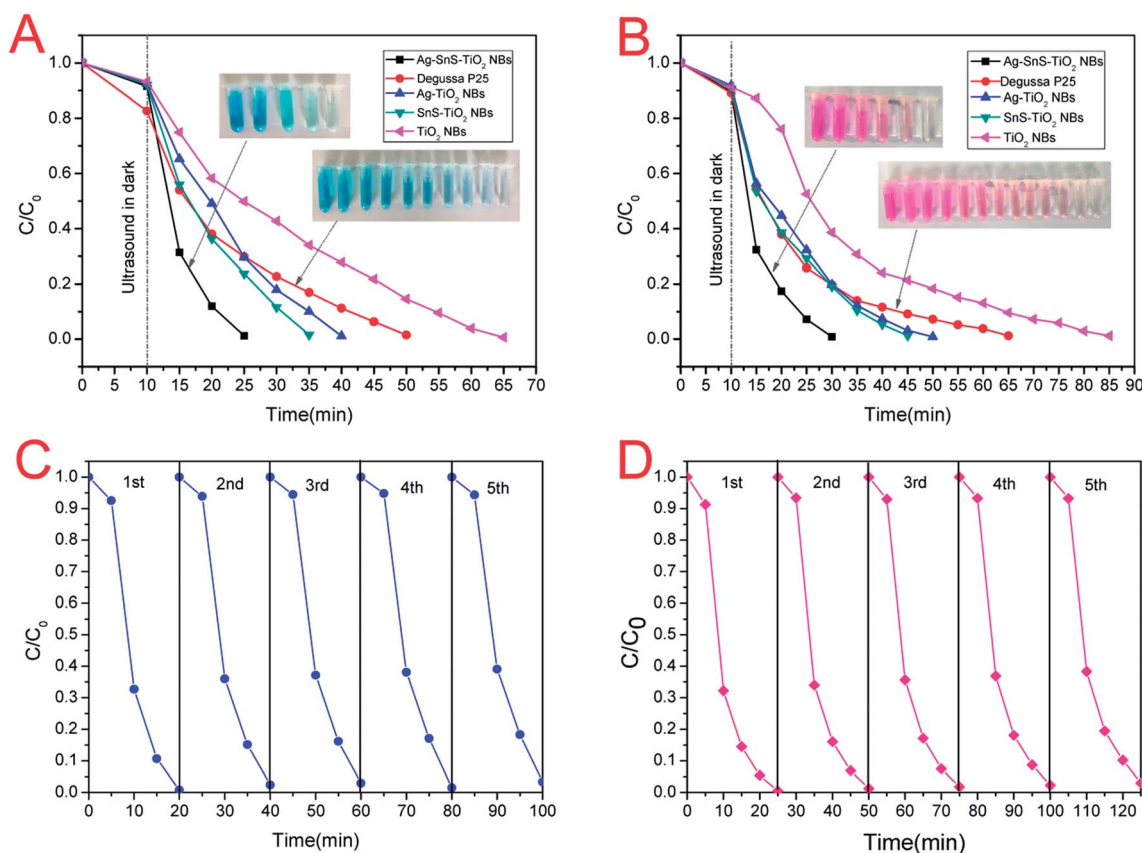

Fig. 6 PC degradation curves of (A) MB and (B) HRB under simulated sunlight. The repeated photocatalytic decomposition of (C) MB and (D) HRB for the Ag–SnS–TiO_2 NBs photocatalyst.

corresponded to Ag 3d3/2 and Ag 3d1/2, respectively. The BE between Ag 3d3/2 and Ag 3d1/2 is 6.0 eV, indicating the formation of Ag nanoparticles in the nanocomposite.[30] As shown in Fig. 5D, the signals at 495.0 eV and 486.6 eV were ascribed to Sn 3d3/2 and Sn 3d5/2, respectively. The BE between Sn 3d3/2 and Sn 3d5/2 is 8.4 eV, indicating the normal state of Sn^{2+} in the nanocomposite.[35] As expected, the high-resolution XPS spectra of S 2p and O 1s in (Fig. 5E and F) revealed the presence of the SnS and TiO_2. The interaction between Ti–O–Sn and O–Ag also indicated Ag and SnS particles here should covalently link to the surface of the TiO_2 NBs.[16,29] In contrast, the only two oxygen signals (529.4 eV and 531.0 eV) in Fig. 5G originated from the Ti–O–Ti and O–H, respectively.[29] SnS and Ag

content in the composites obtained from XPS analysis were 3.55% and 2.51%, respectively.

The PC activities of commercial TiO_2 (Degussa, P-25), pristine TiO_2 NBs, Ag–TiO_2 NBs, SnS–TiO_2 NBs, and ternary Ag–SnS–TiO_2 NBs were evaluated by simulating the photodegradation of simulated organic pollutants (MB and HRB) under sunlight. The degradation efficiency of simulated organic pollutants was defined as C/C_0, where C and C_0 represent the pollutants concentration at irradiation time t and pollutants adsorption–desorption equilibrium initial concentration. All the samples were sonicated in the dark for 10 min to get the pollutants adsorption–desorption equilibrium. The photodegradation curves of MB and HRB were shown in Fig. 6. Under
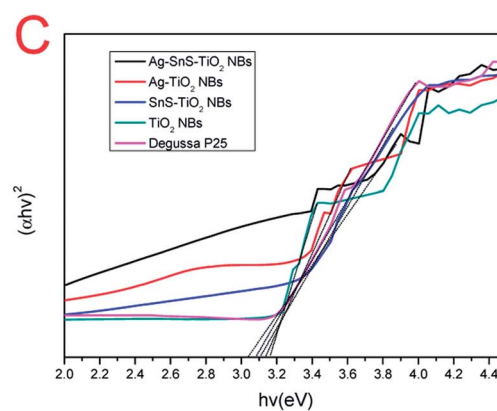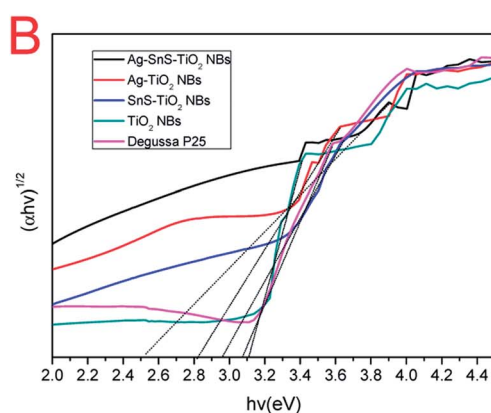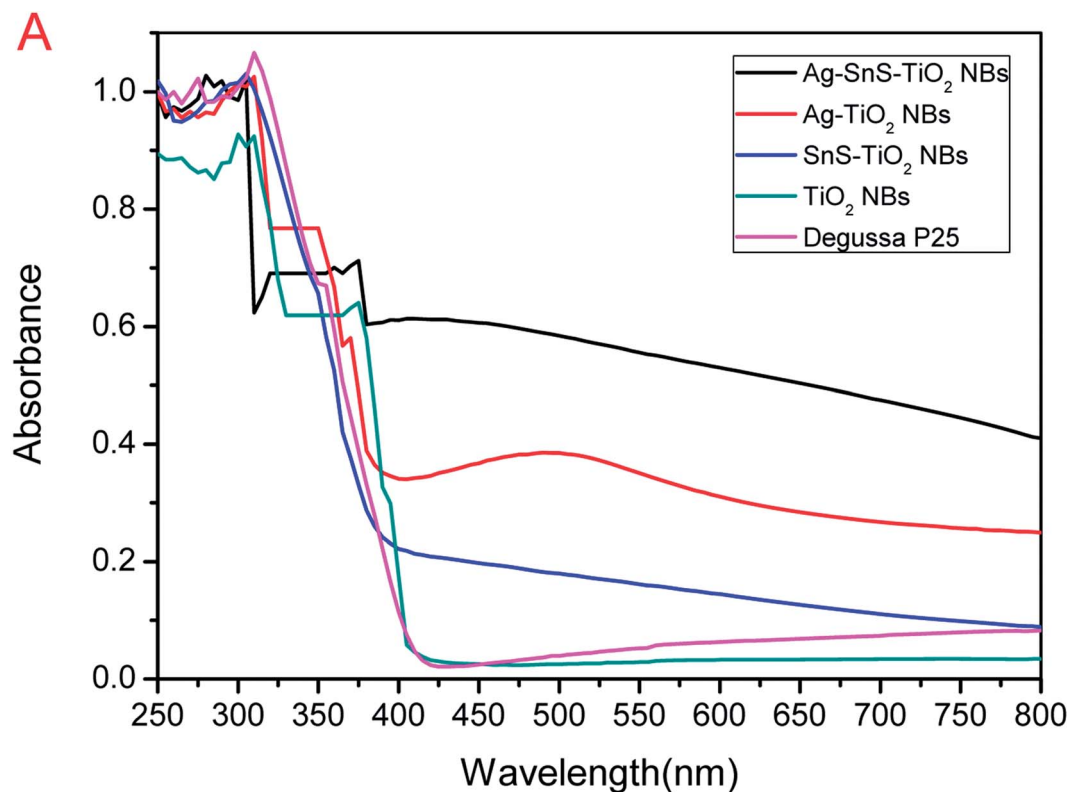

Fig. 7 (A) UV-Vis absorption spectra of TiO_2 NBs, Degussa P25, Ag–TiO_2 NBs, SnS–TiO_2 NBs and Ag–SnS–TiO_2 NBs. (B) $(\alpha h\nu)^{1/2}$ *vs. hν* for TiO_2 NBs, Degussa P25, Ag–TiO_2 NBs, SnS–TiO_2 NBs and Ag–SnS–TiO_2 NBs. (C) $(\alpha h\nu)^2$ *vs. hν* for TiO_2 NBs, Degussa P25, Ag–TiO_2 NBs, SnS–TiO_2 NBs and Ag–SnS–TiO_2 NBs.
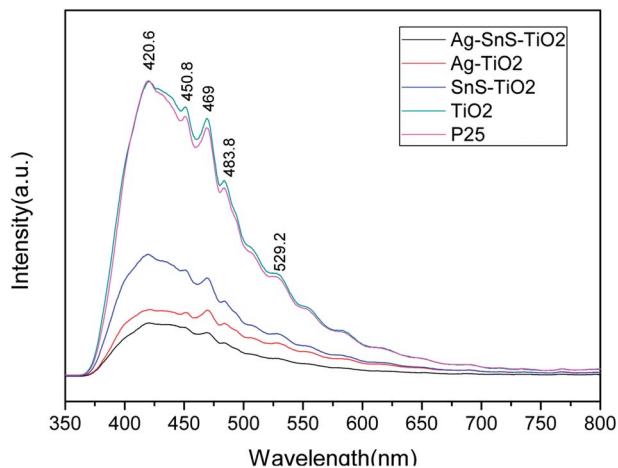
Fig. 8 Photoluminescence spectra of TiO_2 NBs, Degussa P25, Ag–TiO_2 NBs, SnS–TiO_2 NBs and Ag–SnS–TiO_2 NBs.

the photo-induced degradation, the colored aqueous solution turned colorless with the time increase (the inset image of Fig. 6). Notably, the system with ternary Ag–SnS–TiO_2 NBs exhibited the fastest photodegradation, compared to other control photocatalysts systems. In details, MB were fully degraded within 15 min under simulated sunlight irradiation, while Degussa P25 takes about 35 minutes to reach the same level (Fig. 6A). Similarly, Ag–SnS–TiO_2 NBs also exhibited high PC activity against HRB (Fig. 6B) in 20 minutes. In summary, the PC activity of Ag–SnS–TiO_2 NBs is several times faster than that of other control photocatalysts systems, owing to the synergetic effects of Ag and SnS nanoparticles. To investigate the stability of both material and performance of Ag–SnS–TiO_2 NBs as a visible-light photocatalyst, we repeated the photocatalytic decolorization of MB and RHB five times and the corresponding results are shown in Fig. 6C and D. The as-prepared Ag–SnS–TiO_2 NBs can maintain a stable and efficient photocatalytic performance after the first-cycle test, although the photocatalytic activity of repeated cycles was slight decreased compared with the first-cycle result.

Fig. 7A displayed the UV-Vis absorption spectra of the prepared photocatalysts. The deposition of Ag and SnS nanoparticles significantly broadened the absorption rage of TiO_2 NBs into the visible region, which may be attributed to the narrow band gap of SnS nanoparticles and the local surface plasmon resonance of Ag nanoparticles.[15,19,21,36] Furthermore, Ag–SnS–TiO_2 NBs exhibited the highest absorption intensity in the range of 350–800 nm due to the synergistic effect induced by SnS and Ag nanoparticles. Single nanoparticles loaded binary nanocomposites (SnS–TiO_2 NBs and Ag–TiO_2) NBs absorbed visible light much more strongly than unloaded TiO_2 NBs and commercial Degussa P25 in the wavelength range of 400–750 nm, which was consistent with the previous literatures.[6,37] It is obvious that the loading of SnS and Ag nanoparticles remarkably extended the absorption rage into the visible region, significantly improving the light efficiency utilization. The band gaps (E_g) of the synthesized photocatalysts were calculated

from the UV-Vis absorption spectrum.[38] The band gap energies of Ag–SnS–TiO_2 NBs, SnS–TiO_2 NBs, Ag–TiO_2 NBs, Degussa P25 and TiO_2 NBs determined by intercept were about 2.51, 2.82, 2.96, 3.08 and 3.11 eV (Fig. 7B), respectively. Unloaded TiO_2 NBs and Degussa P25 possessed the highest band gaps, in the rage from 3.0 eV to 3.2 eV. The high band gaps were probably due to the presence of rutile phase (3.0 eV) and anatase phase (3.2 eV) in TiO_2 NBs, indirectly consistent with XRD results. Remarkable decrease of the corresponding band gap energy value was attributed to the coupling of Ag and SnS nanoparticles with TiO_2 NBs. The direct band gap of Ag–SnS–TiO_2 NBs, SnS–TiO_2 NBs, Ag–TiO_2 NBs, P25 and TiO_2 NBs was 3.04, 3.08, 3.11, 3.14 and 3.17 eV (Fig. 7C), respectively. There were no significant differences in the value of direct band gap between the groups. It indicates that the improvement in visible-light absorption can be ascribed to the significant decrease of indirect band gap. A Schottky junction formed between Ag nanoparticles and TiO_2 NBs resulted in electrons transferring from the excited TiO_2 NBs to the Ag nanoparticles.[19] Consequently, the electron accumulation induced the Fermi level of Ag nanoparticles shift to the conduction band of TiO_2 NBs, further diminishing the band gap energy of the nanocomposites.[19] Besides, the introduction of narrow-banded SnS nanoparticles could also reduce the band gap of modified TiO_2 NBs. The similar decrease on SnS–TiO_2 heterostructures was also reported by Masahiro Miyauchi et al.[39]

PL emission spectra were performed to characterize the efficiency of charge carrier trapping, transfer, and separation in photocatalysts. As shown in Fig. 8, all the photocatalysts emitted strong signals at 421, 451, 469, 484 and 492 nm. The high-energy peak at 421 nm may be associated with band edge excitation of TiO_2, while the lower energy peaks at 451, 469, 484 and 492 nm were attributed to the oxygen vacancies forming at the surface of Ag–SnS–TiO_2 NBs.[40–42] It is generally believed that PL intensity is inverse related with efficiency of charge carrier separation.[40] Based on our tests, the PL intensity order was as follow: Ag–SnS–TiO_2 NBs < Ag–TiO_2 NBs < SnS–TiO_2 NBs < Degussa P25 < TiO_2 NBs. Therefore, ternary Ag–SnS–TiO_2 NBs exhibited the lowest recombination rate of photoinduced electrons (e^-) and holes (h^+).

To explore the impact of electron (e^-) and hole (h^+) on photodegradation, a comparative experiment were performed as shown in Fig. 9. In our experiment, ethanol and CCl_4 were utilized as hole-trapping and electron-trapping agents, respectively. With the addition of ethanol, the photodegradation efficiency of ternary Ag–SnS–TiO_2 NBs decreased gradually; therein, only half of the MB is degraded in 50 min (Fig. 9A). However, with the addition of CCl_4, photodegradation efficiency happened more quickly; MB was completely degraded in 10 min. Similar results for RHB photodegradation in Fig. 9B were consistent with that for MB. The comparative experiment demonstrated that hole (h^+) played a dominant role in the photodegradation of MB and RHB by Ag–SnS–TiO_2 NBs.[36] Besides, the interaction between Ag–SnS–TiO_2 NB heterostructures functions as an "electron capture agent" to accelerate
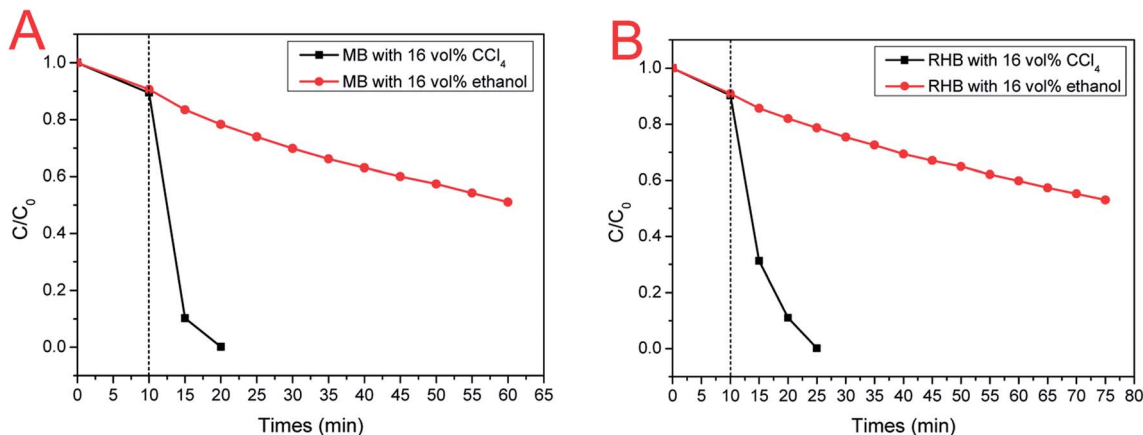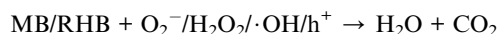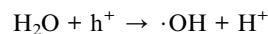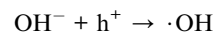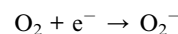
Fig. 9 (A) Photodegradation curves of MB with electron (e^-) or hole (h^+) capture agents; (B) Photodegradation curves of RHB with electron (e^-) or hole (h^+) capture agents. Black curve: 20 mL ethanol was added to 100 mL of aqueous pollutant solution; red curve: 20 mL CCl_4 was added to 100 mL of aqueous pollutant solution.

the photodegradation, similar to CCl_4 in comparative experiments.

We proposed a possible reaction mechanism of MB/RHB photodegradation on ternary Ag–SnS–TiO$_2$ NBs (Fig. 10). Upon exposure to the simulated sunlight, electron–hole pairs are generated in the two excitation semiconductors, TiO$_2$ and SnS. Three possible ways for electron transfer are proposed in this system. First, due to the potential difference between the conduction band of the TiO$_2$ NBs and the Fermi level of the Ag nanoparticle, the excited electrons can transfer from the conduction band of the TiO$_2$ band to the Ag nanoparticles.[19] Second, since the edge of the conduction band of SnS nanoparticle is more negative than that of TiO$_2$, the mobilizing electrons tend to move from the conduction band of SnS nanoparticle to the conduction band of TiO$_2$ NBs.[39] Third, due to the large difference in work function between Ag and SnS, photogenerated electrons are directly implanted into Ag nanoparticles from the conduction band of SnS nanoparticle.[43] Therefore, the ternary Ag–SnS–TiO$_2$ NBs can effectively separate photogenerated electron–hole pairs and delay the carrier recombination. The captured electrons on the Ag nanoparticles can be effectively transferred to the adsorbed oxygen molecules to form superoxide radicals (O_2^-), which can be further converted into hydrogen peroxide (H_2O_2) by reacting with two protons. Meanwhile, the left holes can be reduced by contaminants or rapidly consumed by adsorbed hydroxyl ions or water

molecules, generating hydroxyl radicals ($\cdot$OH). As very strong oxidants, these actives oxidize organic molecules to inorganic compounds that are harmless to the environment.[4,6,44] Therefore, we can conclude that the complex Ag–SnS–TiO$_2$ structure promotes the formation of active species during the PC reaction, resulting in high PC activity. The PC reaction mechanism of Ag–SnS–TiO$_2$ NBs for decomposition of MB/RHB can be summarized as follows:

$$Ag/SnS/TiO_2 \ NBs \xrightarrow{h\nu} e^- + h^+$$

$$O_2 + e^- \rightarrow O_2^-$$

$$O_2^- + 2H^+ \rightarrow H_2O_2$$

$$OH^- + h^+ \rightarrow \cdot OH$$

$$H_2O + h^+ \rightarrow \cdot OH + H^+$$

$$MB/RHB + O_2^-/H_2O_2/\cdot OH/h^+ \rightarrow H_2O + CO_2$$

4. Conclusion

In conclusion, new ternary Ag–SnS–TiO$_2$ NBs composites have been successfully fabricated from natural assembly by using TiO$_2$ nanobelts as templates. Optical absorption, PL and PC activity measurements show that the incorporation of Ag and SnS nanoparticles not only broadens the light absorption rage of TiO$_2$ NBs into the visible region, but also enhances the PC degradation by improving charge transfer through interfacial charge transfer. The PC activity of Ag–SnS–TiO$_2$ NBs photocatalysts is about 2–3 times than that of commercial P25. We hope this work will pave the way for further developing TiO$_2$-based photocatalysts with high the solar energy conversion efficiency.
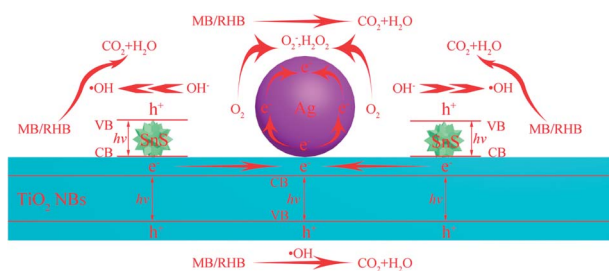

Fig. 10 Schematic representation of photocatalysis mechanism.

Conflicts of interest

There are no conflicts to declare.

Acknowledgements

References

1 O. Edenhofer, K. Seyboth, F. Creutzig and S. Schlömer, *Annu. Rev. Environ. Resour.*, 2013, **38**, 169–200.

2 D. Mitoraj and H. Kisch, *Angew. Chem., Int. Ed.*, 2008, **47**, 9975–9978.

3 Y. Xia, P. Yang, Y. Sun, Y. Wu, B. Mayers, B. Gates, Y. Yin, F. Kim and H. Yan, *Adv. Mater.*, 2003, **15**, 353–389.

4 R. Asahi, T. Morikawa, H. Irie and T. Ohwaki, *Chem. Rev.*, 2014, **114**, 9824–9852.

5 L. Wang and T. Sasaki, *Chem. Rev.*, 2014, **114**, 9455–9486.

6 J. Schneider, M. Matsuoka, M. Takeuchi, J. Zhang, Y. Horiuchi, M. Anpo and D. W. Bahnemann, *Chem. Rev.*, 2014, **114**, 9919–9986.

7 Q. Wang, J. He, Y. Shi, S. Zhang, T. Niu, H. She, Y. Bi and Z. Lei, *Appl. Catal., B*, 2017, **214**, 158–167.

8 S. Sun, P. Gao, Y. Yang, P. Yang, Y. Chen and Y. Wang, *ACS Appl. Mater. Interfaces*, 2016, **8**, 18126–18131.

9 D. Yang, Y. Sun, Z. Tong, Y. Tian, Y. Li and Z. Jiang, *J. Phys. Chem. C*, 2015, **119**, 5827–5835.

10 N. Zhang, Y. Zhang, X. Pan, M.-Q. Yang and Y.-J. Xu, *J. Phys. Chem. C*, 2012, **116**, 18023–18031.

11 Y. Lixia, L. Shenglian, L. Yue, X. Yan, K. Qing and C. Qingyun, *Environ. Sci. Technol.*, 2010, **44**, 7641–7646.

12 Q. Wang, T. Niu, L. Wang, C. Yan, J. Huang, J. He, H. She, B. Su and Y. Bi, *Chem. Eng. J.*, 2017, **337**, 506–514.

13 Y. Chen, G. Zhu, M. Hojamberdiev, J. Gao, R. Zhu, C. Wang, X. Wei and P. Liu, *J. Hazard. Mater.*, 2018, **344**, 42–54.

14 H. Li, J. Ji, X. Zheng, Y. Ma, Z. Jin and H. Ji, *Mater. Sci. Semicond. Process.*, 2015, **36**, 65–70.

15 A. Umar, M. S. Akhtar, R. I. Badran, M. Abaker, S. H. Kim, A. Al-Hajry and S. Baskoutas, *Appl. Phys. Lett.*, 2013, **103**, 101602.

16 Y. Jia, F. Yang, F. Cai, C. Cheng and Y. Zhao, *Electron. Mater. Lett.*, 2013, **9**, 287–291.

17 J. Fang, L. Xu, Z. Zhang, Y. Yuan, S. Cao, Z. Wang, L. Yin, Y. Liao and C. Xue, *ACS Appl. Mater. Interfaces*, 2013, **5**, 8088–8092.

18 N. Roy, K. T. Leung and D. Pradhan, *J. Phys. Chem. C*, 2015, **119**, 19117–19125.

19 Y. Yang, J. Wen, J. Wei, R. Xiong, J. Shi and C. Pan, *ACS Appl. Mater. Interfaces*, 2013, **5**, 6201–6207.

20 M. Maicu, M. C. Hidalgo, G. Colón and J. A. Navío, *J. Photochem. Photobiol., A*, 2011, **217**, 275–283.

21 S. T. Kochuveedu, D.-P. Kim and D. H. Kim, *J. Phys. Chem. C*, 2012, **116**, 2500–2506.

22 A. A. Ismail, D. W. Bahnemann and S. A. Al-Sayari, *Appl. Catal., A*, 2012, **431–432**, 62–68.

23 W. Zhou, G. Du, P. Hu, Y. Yin, J. Li, J. Yu, G. Wang, J. Wang, H. Liu, J. Wang and H. Zhang, *J. Hazard. Mater.*, 2011, **197**, 19–25.

24 Q. Lu, Z. Lu, Y. Lu, L. Lv, Y. Ning, H. Yu, Y. Hou and Y. Yin, *Nano Lett.*, 2013, **13**, 5698–5702.

25 Z. Yang, P. Zhang, Y. Ding, Y. Jiang, Z. Long and W. Dai, *Mater. Res. Bull.*, 2011, **41**, 1625–1631.

26 Q. Wang, J. He, Y. Shi, S. Zhang, T. Niu, H. She and Y. Bi, *Chem. Eng. J.*, 2017, **326**, 411–418.

27 K. G. Deepa and J. Nagaraju, *Mater. Sci. Semicond. Process.*, 2014, **27**, 649–653.

28 H. Tsukigase, Y. Suzuki, M.-H. Berger, T. Sagawa and S. Yoshikawa, *J. Nanosci. Nanotechnol.*, 2011, **11**, 1914–1922.

29 Z. Yang, Y. Jiang, Q. Yu, Y. Ding, Y. Jiang, J. Yin and P. Zhang, *J. Mater. Sci.*, 2017, **52**, 13586–13595.

30 Y. Chen, W. Huang, D. He, Y. Situ and H. Huang, *ACS Appl. Mater. Interfaces*, 2014, **6**, 14405–14414.

31 X. Zhang, J. Liu and E. M. J. Johansson, *Nanoscale*, 2015, **7**, 1454–1462.

32 J. Pan, G. Liu, G. Q. Lu and H.-M. Cheng, *Angew. Chem., Int. Ed.*, 2011, **50**, 2133–2137.

33 J. Ning, K. Men, G. Xiao, L. Wang, Q. Dai, B. Zou, B. Liu and G. Zou, *Nanoscale*, 2010, **2**, 1699–1703.

34 I. Kosackia, T. Suzuki, H. U. Anderson and P. Colomban, *Solid State Ionics*, 2002, **149**, 99–105.

35 H. Hu, B. Yang, J. Zeng and Y. Qian, *Mater. Chem. Phys.*, 2004, **86**, 233–237.

36 Y. Liu, G. Zhu, J. Gao, M. Hojamberdiev, R. Zhu, X. Wei, Q. Guo and P. Liu, *Appl. Catal., B*, 2017, **200**, 72–82.

37 Q. Chen, H. Liu, Y. Xin and X. Cheng, *Chem. Eng. J.*, 2014, **241**, 145–154.

38 Q. Zhang, L. Wang, J. Feng, H. Xu and W. Yan, *Phys. Chem. Chem. Phys.*, 2014, **16**, 23431–23439.

39 M. Miyauchi, *Chem. Phys. Lett.*, 2011, **514**, 151–155.

40 Z. Wu, Y. Wang, L. Sun, Y. Mao, M. Wang and C. Lin, *J. Mater. Chem. A*, 2014, **2**, 8223.

41 K. Li, B. Chai, T. Peng, J. Mao and L. Zan, *ACS Catal.*, 2013, **3**, 170–177.

42 M. Nasir, Z. Xi, M. Xing, J. Zhang, F. Chen, B. Tian and S. Bagwasi, *J. Phys. Chem. C*, 2013, **117**, 9520–9528.

43 K. S. Kumar, A. G. Manohari, S. Dhanapandian and T. Mahalingam, *Mater. Lett.*, 2014, **131**, 167–170.

44 Y. Ma, X. Wang, Y. Jia, X. Chen, H. Han and C. Li, *Chem. Rev.*, 2014, **114**, 9987–10043.